



## Hydrogen storage behavior of nanocrystalline and amorphous La–Mg–Ni-based LaMg<sub>12</sub>-type alloys synthesized by mechanical milling

Yang-huan ZHANG<sup>1,2</sup>, Long-wen LI<sup>1,2</sup>, Dian-chen FENG<sup>1,3</sup>, Peng-fei GONG<sup>1,2</sup>, Hong-wei SHANG<sup>2</sup>, Shi-hai GUO<sup>2</sup>

1. Key Laboratory of Integrated Exploitation of Baiyun Obo Multi-metal Resources,  
Inner Mongolia University of Science and Technology, Baotou 014010, China;

2. Department of Functional Material Research, Central Iron and Steel Research Institute, Beijing 100081, China;

3. School of Materials Science and Engineering, University of Science and Technology Beijing, Beijing 100083, China

Received 4 January 2016; accepted 17 May 2016

**Abstract:** Nanocrystalline and amorphous LaMg<sub>11</sub>Ni+x% Ni (x=100, 200, mass fraction) alloys were synthesized by mechanical milling. The electrochemical hydrogen storage properties of the as-milled alloys were tested by an automatic galvanostatic system. The gaseous hydrogen absorption and desorption properties were investigated by Sievert's apparatus and differential scanning calorimeter (DSC) connected with a H<sub>2</sub> detector. The results indicated that increasing Ni content significantly improves the gaseous and electrochemical hydrogen storage performances of the as-milled alloys. The gaseous hydrogen absorption capacities and absorption rates of the as-milled alloys have the maximum values with the variation of the milling time. But the hydrogen desorption kinetics of the alloys always increases with the extending of milling time. In addition, the electrochemical discharge capacity and high rate discharge (HRD) ability of the as-milled alloys both increase first and then decrease with milling time prolonging.

**Key words:** Ni–MH battery; hydrogen storage alloy; mechanical milling; discharge capacity; kinetics

### 1 Introduction

Developing hydrogen fuel cell vehicles is considered to be an effective and practicable way to fundamentally reduce both energy consumption and carbon dioxide emissions due to the fact that one quarter of the world total energy was consumed by transport [1]. An authoritative survey report from the Ministry of Environmental Protection of China confirmed that automobile exhaust is the main culprit giving rise to a severe haze in Beijing. Therefore, finding new and clean energy alternatives has been highly urgent. Hydrogen, a globally accepted clean and recyclable fuel, has received numerous research attentions due to its high safety and volumetric energy density [2]. A key technical obstacle for the realization of onboard fuel-cell or hydrogen fueled vehicles is to develop a practical hydrogen storage system [3]. Among hydrogen storage methods, hydrogen storage in metal hydrides is considered to be one of the most promising alternatives to satisfy the requirements for mobile application [4]. Several hydrogen storage

materials have been reported for the application goal, yet unfortunately none of them can satisfy all the requirements of the performance proposed by U.S. Department of Energy (DOE) for vehicular applications [5,6]. Regarding hydrogen absorption capacity, Mg-based alloys are considered to be a promising candidate for hydrogen fuel cell vehicles. In particular, REMg<sub>12</sub>-type Mg-based metallic hydrides are looked upon as one of the most promising hydrogen storage materials applied in hydrogen fuel cell vehicles or negative electrodes in Ni–MH batteries because of their gaseous hydrogen storage capacity of 3.7%–6.0% (mass fraction) [7] and theoretical electrochemical capacity of over 1000 mA·h/g [8], much higher than that of Mg–Ni alloys. However, the practical application of the alloys is severely hindered by their relatively high hydrogen desorption temperatures, sluggish hydriding/dehydriding kinetics, extremely low electrochemical discharge capacity at room temperature and quite poor cycle stability either as the hydrogen storage materials of on-board use or as the negative electrode materials of Ni–MH batteries. Therefore, how to improve the

hydrogen storage kinetics of Mg-based alloys is still a major challenge faced by researchers in this area.

On the whole, the primary principles for improving the hydrogen storage kinetics of Mg-based alloys are believed to be no more than two categories: the first one is preparing an ultra-fine microstructure (sub 100 nm range), and the second one is adding catalytic elements such as transition metals, transition metal oxides and rare-earth (RE) metals [9,10]. Some techniques, including 1) mechanical milling [11], 2) rapid solidification (RS) [12], 3) physical vapor deposition [13], 4) hydriding combustion synthesis [14] and 5) equal channel angular pressing (ECAP) [15,16], were successfully applied to synthesizing amorphous and nanocrystalline Mg-based alloys with different compositions. Mechanical milling and melt spinning, in particular, are universally accepted techniques for obtaining amorphous and/or nanocrystalline alloys with a very homogeneous element distribution. WANG et al [17] investigated the electrochemical hydrogen storage properties of ball-milled  $\text{MmMg}_{12}$  alloy with Ni powders, and the results indicated that the first discharge capacity of the ball-milled sample was enhanced from 770 to 1200 mA·h/g by increasing Ni content in the alloy from 150% to 200%. ZHANG et al [18] reported that the as-spun  $\text{Mg}_{10}\text{NiR}$  (R=La, Nd and Sm) alloys displayed superior hydriding and dehydriding kinetics, the remarkable improvement of which was ascribed to adding different rare earth elements. YARTYS et al [19] reported that the  $\text{LaMg}_{11}\text{Ni}$  alloy solidified at the highest cooling rate exhibited the fastest hydrogenation kinetics, reaching maximum hydrogenation capacity of 5.02% H.

It is well known that Ni can accelerate the amorphization process in the alloy and exert a very powerful catalytic action for the hydrogen absorption and desorption of Mg-based alloys. In addition, Ni has a good corrosion resistance to an alkaline solution. Hence, in the present work, Mg in the  $\text{LaMg}_{12}$ -type alloy was partially substituted by Ni. The nanocrystalline and amorphous  $\text{LaMg}_{11}\text{Ni}+x\%\text{Ni}$  ( $x=100, 200$ ) alloys were prepared by mechanical milling, and the effects of Ni content and milling time on the gaseous and electrochemical hydrogen storage performance of the alloys were investigated in detail.

## 2 Experimental

$\text{LaMg}_{11}\text{Ni}$  experimental alloys were prepared by using a vacuum induction furnace under a helium atmosphere and at a pressure of 0.04 MPa to prevent Mg from volatilization. The molten alloy was poured into a cooled copper mould and then a cast ingot was obtained. The as-cast alloys were mechanically crushed into powder with a diameter of about 50  $\mu\text{m}$ . The alloy

powder was mixed with carbonyl nickel powder with a mass ratio of 1:1 and 1:2, respectively. Then, the mixed powder was mechanically milled by a planetary-type mill in an argon atmosphere to prevent the powder from oxidation during ball milling. The samples were handled in a glove box under Ar. Cr–Ni stainless steel ball and the powder with a mass ratio of 35:1 were put into Cr–Ni stainless steel vials together. The milling speed was 350 r/min and the duration time was 5, 10, 20, 40 and 60 h, respectively. For simplicity, the chemical composition of ball-milled alloys was defined as  $\text{LaMg}_{11}\text{Ni}+x\%\text{Ni}$  ( $x=100, 200$ ). All gaseous hydrogen sorption capacities and electrochemical performances of the samples were calculated based on  $\text{NdMg}_{11}\text{Ni}$  (excluding the mass of carbonyl nickel powder during ball milling) alloy.

The phase structures of the as-cast and milled alloys were determined by X-ray diffraction (XRD) (D/max/2400). The diffraction, with the experimental parameters of 160 mA, 40 kV and 10 ( $^\circ$ )/min, respectively, was performed with Cu  $K_\alpha$  radiation filtered by graphite. The powder samples of the as-milled alloys were observed by high resolution transmission electron microscope (HRTEM) (JEM–2100F, operated at 200 kV) and their crystalline states were ascertained by electron diffraction (ED).

The hydrogen absorption and desorption kinetics of these alloys was measured using an automatically controlled Sievert's apparatus with a furnace controlled to an accuracy of  $\pm 1$  K. An initial hydrogen pressure of 3 MPa was applied to inducing hydrogen absorption of the alloy particles at the temperatures of 553, 573, 593 and 613 K as well as hydrogen desorption at a pressure of  $1 \times 10^{-4}$  MPa at the same temperatures. 300 mg sample was loaded into a cylindrical reactor for each measurement. Hydrogen desorption properties were also measured using a differential scanning calorimeter (DSC, STA449C) at heating rates of 5, 10, 15 and 20 K/min.

The electrochemical kinetics was measured at 303 K by using a three-electrode open cell consisting of a working electrode (the metal hydride electrode), a sintered  $\text{Ni}(\text{OH})_2/\text{NiOOH}$  counter electrode as well as a Hg/HgO reference electrode, which were immersed in 6 mol/L KOH electrolyte. The metal hydride electrodes were prepared by pressing 0.200 g of ball-milled alloy powders and 0.800 g of carbonyl nickel powders into pellets with 10 mm in diameter under 25 MPa pressure. Carbonyl nickel powder served as the frame of the pellet and current collector. The electrochemical properties of the alloy electrodes were determined using an automatic battery test instrument (LAND, CT2001A). The voltage between the negative and the reference electrodes was defined as the discharge voltage. In every cycle, the alloy electrode was firstly charged at a constant current

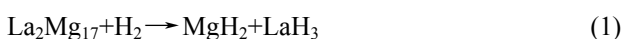
density. After resting for 15 min, it was discharged at the same current density to the cut-off voltage of  $-0.500$  V. For the high rate discharge (HRD) ability of the alloy electrodes, they were charged at  $60$  mA/g for  $20$  h and then discharged at different discharge current densities ( $60, 300, 600, 900,$  and  $1200$  mA/g) to the cut-off cell voltage of  $0.500$  V (vs  $-Hg/HgO$ ) after a  $15$  min rest.

The electrochemical impedance spectra (EIS) were measured at different temperatures using an electrochemical workstation (PARSTAT 2273). The fresh electrodes were fully charged and then rested for  $2$  h up to the stabilization of the open circuit potential. The EIS of the alloy electrodes was measured at a  $50\%$  depth of discharge (DOD), within the frequency ranging from  $10$  kHz to  $5$  mHz, the amplitude of signal potentiostatic or galvanostatic measurements being  $5$  mV, and the number of points per decade of frequencies being  $60$ . For the potentiostatic discharge, the test electrodes in the fully charged state were discharged at  $500$  mV potential steps for  $5000$  s on the electrochemical workstation, using electrochemistry corrosion software (CorrWare).

### 3 Results and discussion

#### 3.1 Microstructure characteristics

The phase components and structural characteristics of the as-cast and milled  $LaMg_{11}Ni+x\%$  Ni ( $x=0, 100, 200$ ) alloys before and after hydriding were subjected to XRD detections, just as shown in Fig. 1. It reveals that the as-cast  $LaMg_{11}Ni$  alloy possesses biphasic structures with a major phase  $La_2Mg_{17}$  and a secondary phase  $Mg_2Ni$ . The mechanical milling results in the merging and broadening of the diffraction peaks with increasing Ni content, indicating that the crystalline structure has transformed to a nanocrystalline or amorphous structure. Furthermore, increasing Ni content in alloys makes the intensity of diffraction peaks evidently lower and its width clearly broaden. That is to say, increasing Ni content facilitates the glass forming of the alloy. As stated by ABDELLAOUI et al [20], increasing Ni content can also lower the activation energy for the crystalline to amorphous phase transformation of  $REMg_{12}$  alloys. After hydriding, we can observe three hydrides in the as-cast alloy, including  $LaH_3$ ,  $MgH_2$  and  $Mg_2NiH_4$ , which originate from the following reactions [21]:



We also note that after hydriding, the diffraction peaks of the as-cast and milled alloys obviously broaden, which results from the lattice stress and expansion when hydrogen atoms enter the lattice interstitials of the alloys. The as-milled  $LaMg_{11}Ni+x\%$  Ni ( $x=100, 200$ ) alloys in a

saturated hydrogen absorption state still exhibit nanocrystalline and amorphous structure, indicating that the as-milled alloys are of a good structure stability.

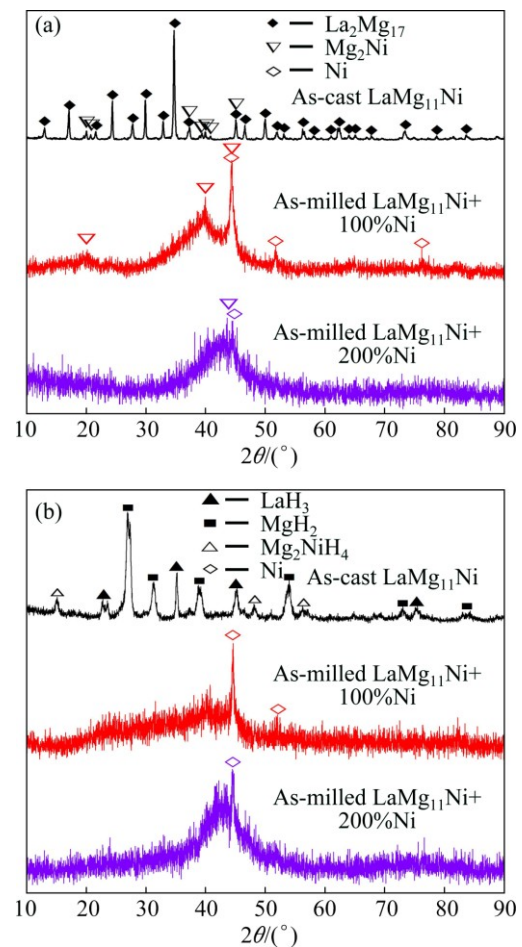


**Fig. 1** XRD profiles of as-cast and milled (40 h)  $LaMg_{11}Ni+x\%$  Ni ( $x=0, 100, 200$ ) alloys before and after hydriding: (a) Before hydriding; (b) After hydriding

Figure 2 shows the HRTEM images and electron diffraction (ED) patterns of the as-cast and milled (40 h)  $LaMg_{11}Ni+x\%$  Ni ( $x=0, 100, 200$ ) alloys. Two phases  $La_2Mg_{17}$  and  $Mg_2Ni$  are found in the as-cast alloy, as shown by the ED pattern. Obviously, after milling for  $40$  h, the  $LaMg_{11}Ni+100\%$  Ni alloy exhibits a major nanocrystalline structure, while the  $LaMg_{11}Ni+200\%$  Ni alloy displays a visible nanocrystalline and amorphous structure, suggesting that increasing Ni content facilitates the glass forming of the  $Mg_2Ni$  alloy during milling, which is also evidenced by TERESIAK et al [22]. The average size of the as-milled alloys measured by linear intercept method is found to be in the range of  $8\text{--}12$  nm. Meanwhile, some crystal defects can be clearly observed in the as-milled alloys.

#### 3.2 Gaseous hydrogen absorption/desorption kinetics

To investigate the absorption kinetics, the hydrogen absorption capacities of the as-milled  $LaMg_{11}Ni+x\%$  Ni

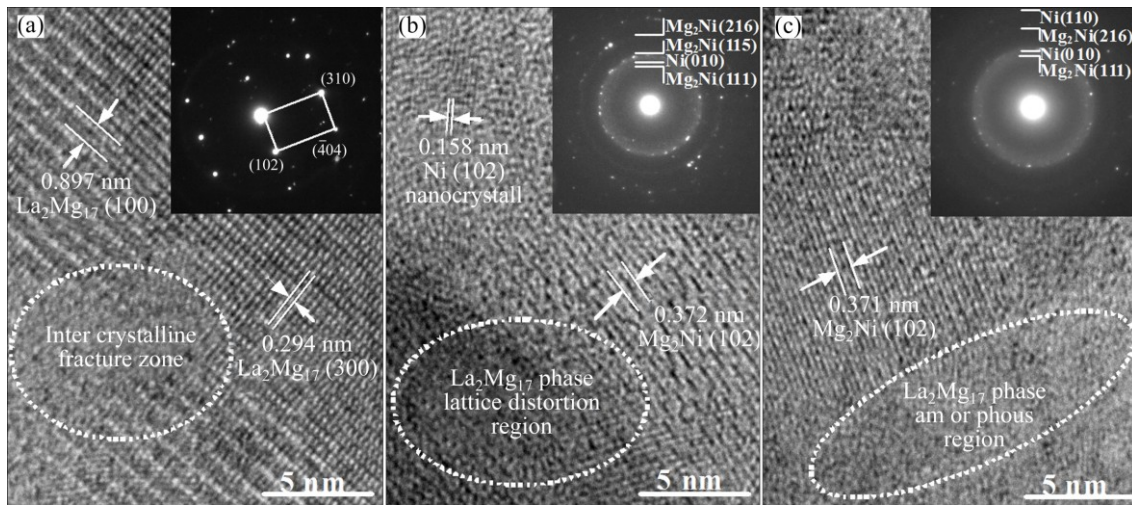


**Fig. 2** HRTEM images and ED patterns of as-cast and milled (40 h)  $\text{LaMg}_{11}\text{Ni}+x\% \text{Ni}$  ( $x=0, 100, 200$ ) alloys: (a)  $x=0$ , as-cast; (b)  $x=100$ , milled for 40 h; (c)  $x=200$ , milled for 40 h

( $x=100, 200$ ) alloys as functions of reaction time are measured at 573 K and 3 MPa  $\text{H}_2$  pressure, as presented in Fig. 3. The as-milled alloys exhibit a very fast hydrogen absorption rate in the initial stage, after that, the hydrogen content is almost saturated at the next quite a long hydrogenation time. In the current experiment, we find that the  $C_{100}^a$  values of all the experimental alloys are more than 98% of their saturated hydrogen absorption capacity. Therefore,  $C_{100}^a$  value can be reasonably considered as the saturated hydrogen absorption capacity of the alloys. The relationship between the  $C_{100}^a$  values of the as-milled alloys and the milling time can be easily established, as depicted in Fig. 3. Evidently, with milling time prolonging, the  $C_{100}^a$  values of the as-milled alloys firstly increase and then decrease. The maximum  $C_{100}^a$  values are 5.915% for the  $\text{LaMg}_{11}\text{Ni}+100\% \text{Ni}$  alloy and 6.171% for the  $\text{LaMg}_{11}\text{Ni}+200\% \text{Ni}$  alloy. Just as hydrogen absorption capacity, hydrogen absorption rate is also extremely important for hydrogen storage materials applied in onboard hydrogen storage system. Here, hydrogen absorption saturation ratio ( $R_t^a$ ) (a ratio of the hydrogen absorption capacity at a fixed time to the saturated hydrogen absorption capacity) is used to represent the hydriding kinetics of hydrogen storage alloys, which is defined as  $R_t^a = C_t^a / C_{100}^a \times 100\%$ , where  $C_t^a$  and  $C_{100}^a$  are hydrogen absorption capacities at  $t$  min and 100 min, respectively. Similarly, hydrogen desorption ratio ( $R_t^d$ ) (a ratio of the hydrogen desorption capacity at a fixed time to the saturated hydrogen absorption capacity) is used to symbolize the hydrogen desorption kinetics of the alloys, which is defined as  $R_t^d = C_t^d / C_{100}^a \times 100\%$ , where  $C_{100}^a$  is the same as the previous one and  $C_t^d$  is the hydrogen desorption capacity in the time of  $t$  min, respectively. For the better possibility of mutual comparison, we take 10 min as a benchmark for

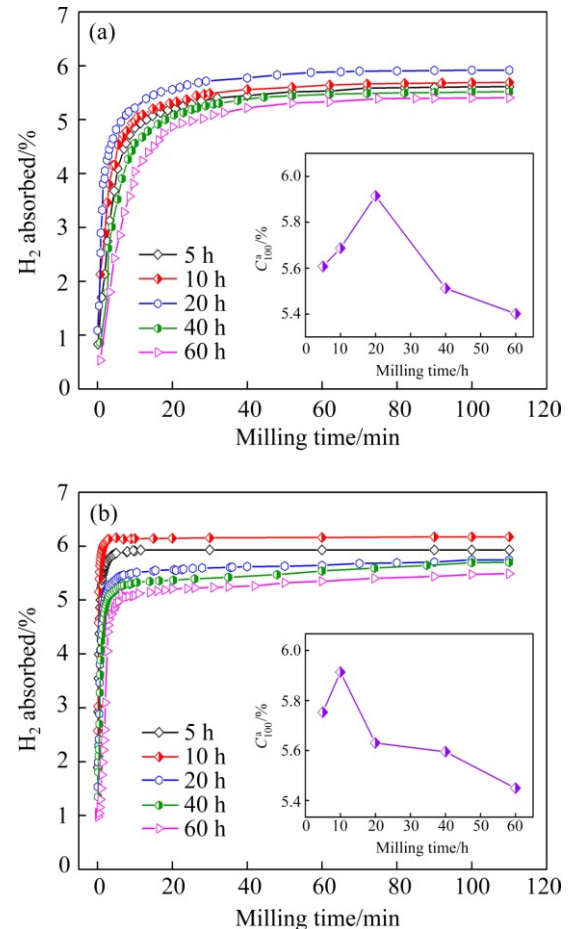


**Fig. 3** Hydrogen absorption kinetic curves of as-milled  $\text{LaMg}_{11}\text{Ni}+x\% \text{Ni}$  ( $x=100, 200$ ) alloys at 573 K: (a)  $x=100$ ; (b)  $x=200$

hydrogen absorption and 20 min for hydrogen desorption. Based on the above mentioned definitions, the relationships between the  $R_{10}^a$  ( $t=10$ ) as well as  $R_{20}^d$  ( $t=20$ ) values of the as-milled  $\text{LaMg}_{11}\text{Ni}+x\% \text{Ni}$  ( $x=100,$

200) alloys and the milling time, are described in Fig. 4. Obviously, the  $R_{10}^a$  values of the as-milled alloys firstly increase and then decrease with the increase of milling time. When the milling time is 20 h for the LaMg<sub>11</sub>Ni+100%Ni alloy and 10 h for the LaMg<sub>11</sub>Ni+200%Ni alloy, the  $R_{10}^a$  values of the LaMg<sub>11</sub>Ni+x% Ni (x=100, 200) alloys reach maximum, namely 88.2% and 99.7%, respectively. Differing from hydrogen absorption kinetics, prolonging milling time always facilitates the dehydrogening kinetics of the alloys. To be specific, extending milling time from 5 to 60 h makes the  $R_{20}^d$  value increase from 20.3% to 27.3% for the LaMg<sub>11</sub>Ni+100%Ni alloy and from 22.5% to 31.8% for the LaMg<sub>11</sub>Ni+200%Ni alloy, respectively. Furthermore, it is noteworthy that, for the same milling time, the LaMg<sub>11</sub>Ni+200%Ni alloy exhibits much higher  $R_{10}^a$  and  $R_{20}^d$  values, indicating that increasing Ni content generates relatively catalytic alloy surface for the hydrogen reactions in the process of ball milling, as stated by ANIK et al [23].

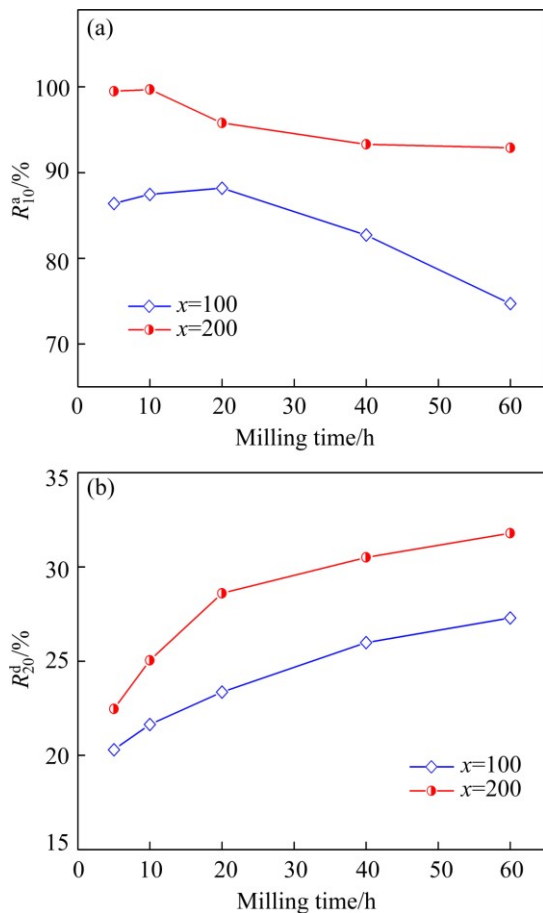


**Fig. 4** Evolutions of  $R_{10}^a$  (a) and  $R_{20}^d$  (b) values of as-milled LaMg<sub>11</sub>Ni+x% Ni (x=100, 200) alloys at 573 K alloys with milling time

Generally, the activation energy is viewed as a crucial parameter for evaluating the gas–solid reaction kinetics. With respect to gaseous hydrogen desorption, it

is usually considered to be associated with total energy barrier concerning hydrogen desorption processes [24]. Hence, we can use the change of activation energy to evaluate the driving force of hydrogen desorption reaction. The activation energy for hydrogen desorption can be commonly estimated by Kissinger method according to the following equation [25]:

$$\frac{d[\ln(\beta/T_p^2)]}{d(1/T_p)} = \frac{-E_k^{de}}{R} \quad (3)$$

where  $E_k^{de}$  is the activation energy,  $\beta$  is the heating rate,  $T_p$  is the absolute temperature corresponding to the maximum desorption rate in the DSC curves, and  $R$  is the mole gas constant (8.314 J/(mol·K)). In order to meet the calculation conditions of Kissinger method, the hydrogen desorption reactions of the as-milled LaMg<sub>11</sub>Ni+x% Ni (x=100, 200) alloys in a saturated hydrogen absorption state at 573 K and 3 MPa are measured by DSC at heating rates of 5, 10, 15 and 20 K/min, as provided in Fig. 5. A clear endothermic peak is observed in correspondence with the hydrogen desorption.

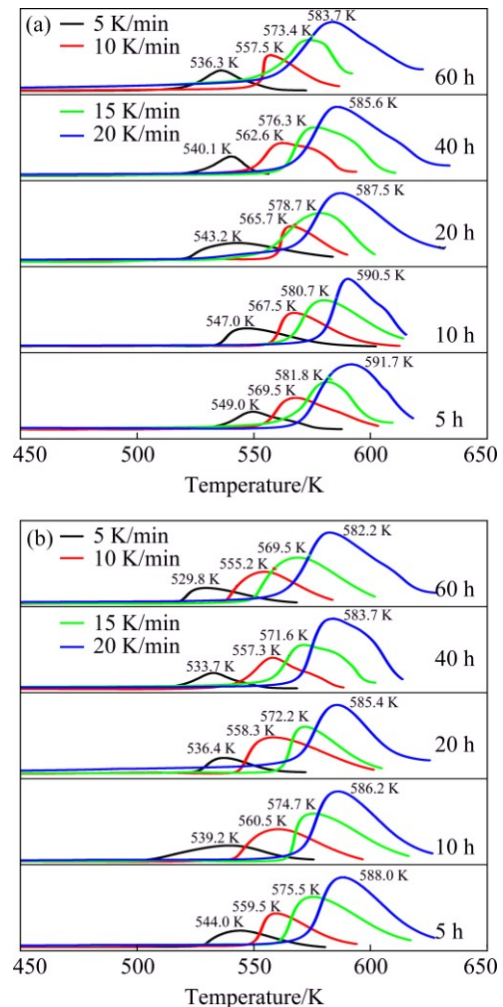


**Fig. 5** DSC curves of as-milled LaMg<sub>11</sub>Ni+x% Ni (x=100, 200) alloys at various heating rates: (a) x=100; (b) x=200

Furthermore, all the alloys are found to display similar peak shapes, suggesting that each reaction involves in the same reaction process. Meanwhile, it is found by comparing Figs. 5(a) and (b) that for each heating rate, the endothermic peak of the LaMg<sub>11</sub>Ni+200%Ni alloy has a drift to low temperatures, implying that the reaction rate was ameliorated by increasing Ni content in the desorption process as well. Based on the data in Fig. 5, the logarithmic transform of the Eq. (3) has been used to establish a graph of  $\ln(\beta/T_p^2)$  vs  $1/T_p$ , namely Kissinger plots, which are found to be approximately linear, as demonstrated in Fig. 6. From the slopes of the Kissinger plots, the activation energy  $E_k^{\text{de}}$  can be easily calculated, and the relationships between the  $E_k^{\text{de}}$  values of the as-milled alloys and the milling time can be easily derived, as inserted in Fig. 6. It can be seen that the  $E_k^{\text{de}}$  values of the as-milled alloys clearly decrease with milling duration extending. More specifically, with milling time increasing from 5 to 60 h, the  $E_k^{\text{de}}$  value decreases from 78.6 to 66.3 kJ/mol for the LaMg<sub>11</sub>Ni+100%Ni alloy and from 71.2 to 59.1 kJ/mol for the LaMg<sub>11</sub>Ni+200%Ni alloy. Based on the above results, it can be concluded that the hydrogen desorption kinetics improved by extending milling time originates from a decrease in the activation energy.

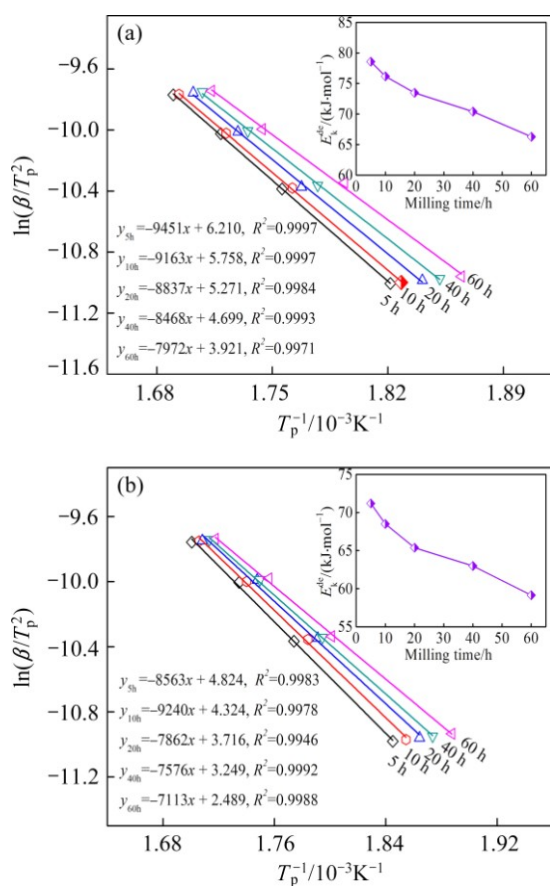


**Fig. 6** Kissinger plots and evolution of  $E_k^{\text{de}}$  values of as-milled LaMg<sub>11</sub>Ni+x%Ni ( $x=100, 200$ ) alloys with milling time: (a)  $x=100$ ; (b)  $x=200$

In consideration of the above-mentioned results, some elucidations can be provided for the effects of Ni content and milling time on the hydrogen absorption and desorption kinetics of the alloys. As for the positive impact of the mechanical milling on hydrogen storage kinetics, it is believed to be associated with the change of the alloy structure resulting from ball milling. The crystalline alloy milled mechanically becomes at least partially disordered and its structure changes into nanocrystalline or amorphous, creating a lot of new crystallites and grain boundaries (Fig. 2), which can provide numerous sites with low diffusion activation energy, facilitating the diffusion of hydrogen atoms in alloys [26]. Here, it is noteworthy that the ball milling for a higher time 20 h for the LaMg<sub>11</sub>Ni+100%Ni alloy or 10 h for the LaMg<sub>11</sub>Ni+200%Ni alloy will incur an undesirable decrease in the hydriding rate of the alloys, which is ascribed to the increase of Ni content facilitating the glass forming due to the fact that the diffusion ability of hydrogen atoms in an amorphous phase is much lower than that in a nanocrystalline phase [27]. As to the beneficial action of increasing milling time on the hydrogen desorption kinetics, it is now well established that reducing the grain size far below the micrometer scale can dramatically improve the dehydrogenation properties of Mg-based alloys [28]. The improved hydrogen absorption and desorption kinetics by increasing Ni content is believed to create relatively catalytic alloy surface for the hydrogen reactions during mechanical milling [29].

### 3.3 Electrochemical hydrogen storage performance

Shown in Fig. 7 are the discharge potential curves of the as-milled LaMg<sub>11</sub>Ni+x%Ni ( $x=100, 200$ ) alloy electrodes with a current density of 60 mA/g at the first charging/discharging cycle, in which  $C_{\text{max}}$  is the maximum discharge capacity of the alloys. All the alloys can be easily activated to reach the maximum capacity at the first cycle. The discharge potential characteristic, which directly determines the stability of the output power, is a very important performance of the alloy electrode and is characterized by the potential plateau of the discharge curve of the alloy. The longer and more horizontal the discharge potential plateau is, the better the discharge potential characteristics of the alloy will be. We note that mechanical milling markedly improves the discharge potential characteristics of the alloys, enhancing discharge potential and lengthening discharge plateau. Meanwhile, it is found that mechanical milling exerts an obvious effect on the discharge capacity of alloys. The milling time dependence of the discharge capacity of the alloys is also inserted in Fig. 7. It is found that, for the milling time of 40 h, increasing Ni content from  $x=100$  to  $x=200$  brings on the discharge capacity of

the alloys growing from 157.3 to 1053.5 mA·h/g. This indicates that increasing Ni content is beneficial to the enhancement of the discharge capacity of the as-milled alloys, which is most likely attributed to the formation of the highly dispersed metallic Ni nanocrystalline through amorphous alloy matrix and the reduction of hydride stability as a result of increasing Ni content [8].

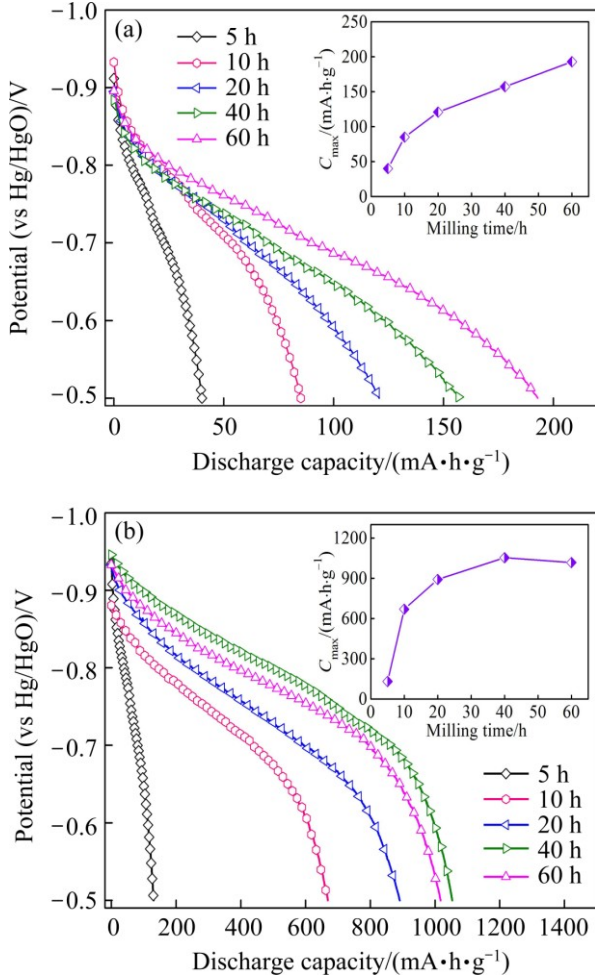


**Fig. 7** Discharge potential curves of as-milled LaMg<sub>11</sub>Ni+x%Ni (x=100, 200) alloys and evolution of discharge capacity of alloys with milling time: (a) x=100; (b) x=200

Generally, the electrochemical kinetics of an alloy electrode is evaluated by its high rate discharge (HRD) ability, which is defined as:  $D_{HR} = C_i / C_{60} \times 100\%$ , where  $D_{HR}$  is the high rate discharge ability,  $C_i$  and  $C_{60}$  are the maximum discharge capacities of the alloy electrode charged– discharged at the current densities of  $J$  and 60 mA/g, respectively. The  $D_{HR}$  values of the as-milled LaMg<sub>11</sub>Ni+x%Ni (x=100, 200) alloys as functions of current density are described in Fig. 8. It can be seen that the as-milled alloys show very good electrochemical kinetics. To facilitate comparison, we take the current density of 600 mA/g ( $J=600$  mA/g) as a criterion to establish the relationships between the  $D_{HR}$  of the as-milled alloys and the milling time, as described in

Figs. 8(a) and (b), respectively. It is found that the  $D_{HR}$  of the as-milled alloys reach maximum values with the variation of the milling time, namely 72.6% for the LaMg<sub>11</sub>Ni+100%Ni alloy milled for 20 h and 75.2% for the LaMg<sub>11</sub>Ni+200%Ni alloy milled for 40 h, which is approximately equal to the electrochemical kinetics of the rare earth-based AB<sub>5</sub>-type alloy electrode possessing acknowledged excellent kinetics performance.

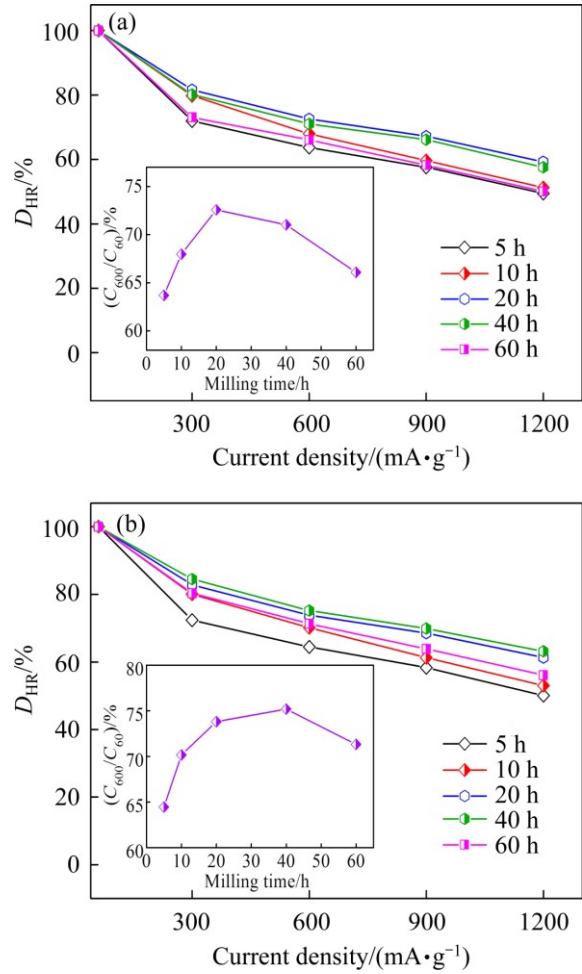


**Fig. 8** Evolution of  $D_{HR}$  of as-milled LaMg<sub>11</sub>Ni+x%Ni (x=100, 200) alloys with current density: (a) x=100; (b) x=200

To reveal the mechanism of the electrochemical kinetics of alloys impacted by varying milling time, the effects of the milling time on the diffusion ability of hydrogen atoms and the charge-transfer rate were investigated due to the fact that the HRD of an alloy electrode is considered to be basically determined by the hydrogen diffusion capability in the alloy bulk and charge-transfer rate on the alloy electrode surface [30]. First, hydrogen diffusion coefficient can be obtained by means of the semilogarithmic curves of anodic current versus the working duration of an alloy electrode, as shown in Fig. 9. Based on the White’s model [31], the diffusion coefficient of the hydrogen atoms in the bulk of the alloy could be calculated easily through the slope of

the linear region of the corresponding plots according to the following formulae:

$$\lg J = \lg \left( \pm \frac{6FD}{da^2} (C_0 - C_s) \right) - \frac{\pi^2}{2.303} \frac{D}{a^2} t \quad (4)$$

$$D = - \frac{2.303a^2}{\pi^2} \frac{d \lg J}{dt} \quad (5)$$

where  $J$  is the diffusion current density (A/g),  $D$  is the hydrogen diffusion coefficient (cm<sup>2</sup>/s),  $C_0$  is the initial hydrogen concentration in the bulk of the alloy (mol/cm<sup>3</sup>),  $C_s$  is the hydrogen concentration on the surface of the alloy particles (mol/cm<sup>3</sup>),  $a$  is the alloy particle radius (cm),  $d$  is the density of the hydrogen storage alloy (g/cm<sup>3</sup>),  $t$  is the discharge time (s), respectively. The  $\pm$  sign in Eq. (4) indicates the charge (–) and discharge (+) processes. The  $D$  values of the alloys derived by Eq. (5) as functions of the milling time are also inserted in Figs. 9(a) and (b), respectively. Apparently, the  $D$  values of the alloys first increase and then decrease with milling time increasing.

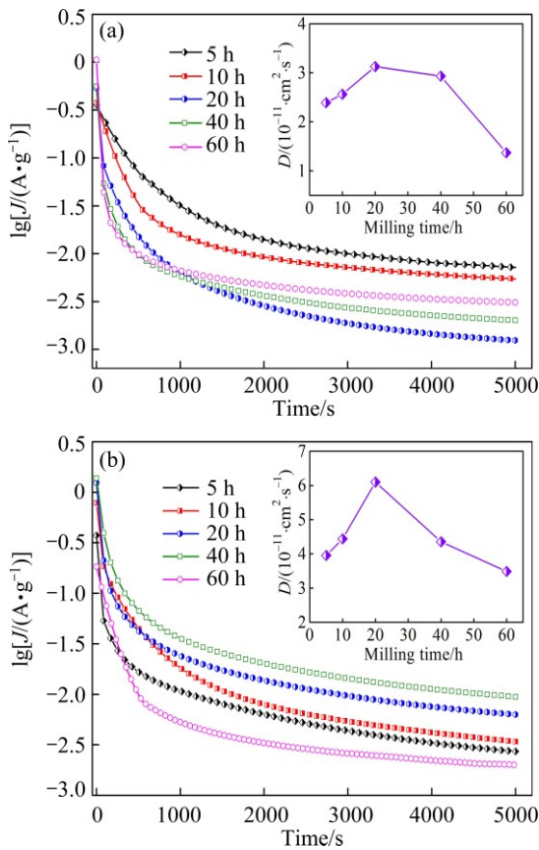


**Fig. 9** Semilogarithmic curves of anodic current vs time responses of as-milled LaMg<sub>11</sub>Ni + x% Ni (x=100, 200) alloys: (a) x=100; (b) x=200

With respect to the charge-transfer capability on the surface of the alloy electrode, it can be qualitatively evaluated by their EIS in view of the Kuriyama's

model [32]. The typical EIS curves obtained at 303 K of the as-milled LaMg<sub>11</sub>Ni+x%Ni (x=100, 200) alloys are shown in Fig. 10. Each EIS curve is found to have two distorted capacitive loops at the high and middle frequency regions separately as well as a line at the low frequency region, which very well represents the electrochemical process of the alloy electrode. Among them, the smaller semicircle in the high frequency region reflects the contact resistance between the alloy powder and the conductive material, and the larger one in the middle frequency region corresponds to the charge-transfer resistance ( $R_{ct}$ ) on the alloy surface while the straight line in the low frequency region corresponds to Warburg impedance. With the equivalent circuit (see Fig. 10(a)), the  $R_{ct}$  values were obtained with the fitting program Z-View, and the result is shown in Fig. 10(b). As considered by KURIYAMA et al [32], the  $R_{ct}$  is determined by both the reactivity of the alloy surface and the reaction area. And the electrochemical reactivity of the alloy surface can be evaluated with apparent activation enthalpy  $\Delta_r H^*$ , which can be obtained by the following equation:

$$\ln(T/R_{ct}) = C_0 - \frac{\Delta_r H^*}{RT} \quad (6)$$

where  $R_{ct}$  is the charge-transfer resistance for the metal hydride electrodes ( $\Omega$ ),  $R$  is the mole gas constant

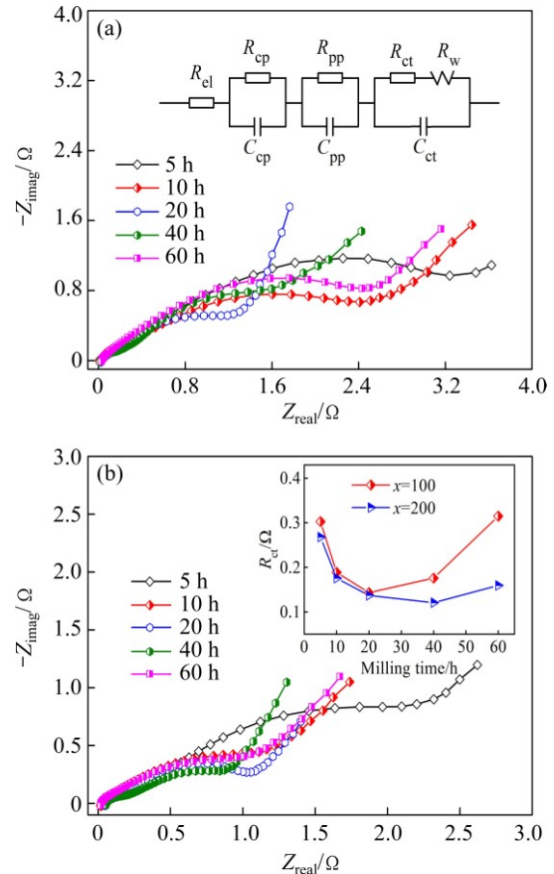


**Fig. 10** Electrochemical impedance spectra (EIS) of as-milled LaMg<sub>11</sub>Ni+x%Ni (x=100, 200) alloys: (a) x=100; (b) x=200

(8.314 J/(mol·K)),  $T$  is the temperature (K) and  $C_0$  is a constant in which the surface area is included. To meet the calculation conditions of Eq. (6), the EIS curves of the as-milled (40 h)  $\text{LaMg}_{11}\text{Ni}+x\%\text{Ni}$  ( $x=100, 200$ ) alloys are measured at different temperatures (303, 313 and 323 K), as illustrated in Fig. 11. Based on the data in Fig. 11, the logarithmic transform of the Eq. (6) has been used to construct a graph of  $\ln(T/R_{ct})$  vs  $1/T$ , namely Kuriyama plots which are found to be approximately linear, as inserted in Fig. 11. From the slopes of the Kuriyama plots, the  $\Delta_r H^*$  values can be easily calculated. The activation enthalpies  $\Delta_r H^*$  of the as-milled (40 h)  $\text{LaMg}_{11}\text{Ni}+x\%\text{Ni}$  ( $x=100, 200$ ) alloys are 14.7 and 10.7 kJ/mol, respectively. The  $\Delta_r H^*$  values of the entire as-milled  $\text{LaMg}_{11}\text{Ni}+x\%\text{Ni}$  ( $x=100, 200$ ) alloys are calculated, and the obtained results are shown in Fig. 12. Obviously, the  $\Delta_r H^*$  values of the alloys firstly decrease and then increase with the milling time extending. By comparing the change trends of the  $D_{HR}$  and  $\Delta_r H^*$  values with the milling time shown in Figs. 8 and 12, we can conclude that the  $\Delta_r H^*$  value is a very important factor affecting the electrochemical kinetics of the alloys.

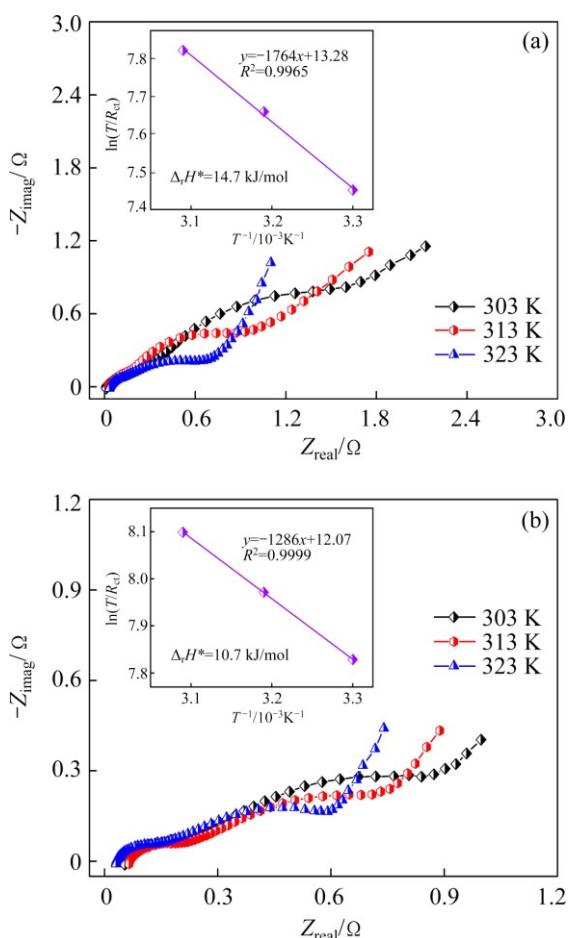


**Fig. 11** Electrochemical impedance spectra (EIS) of as-milled (40 h)  $\text{LaMg}_{11}\text{Ni}+x\%\text{Ni}$  ( $x=100, 200$ ) alloys at various temperatures: (a)  $x=100$ ; (b)  $x=200$

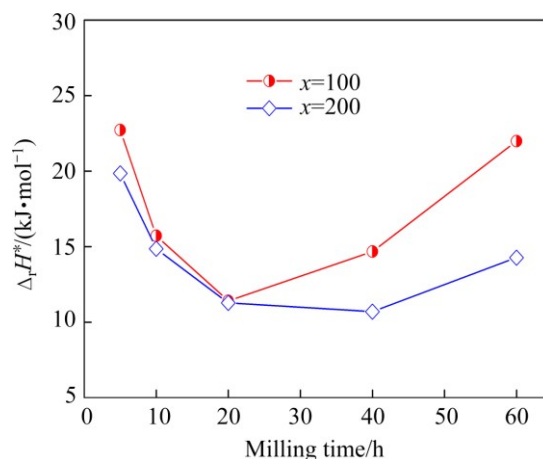


**Fig. 12** Evolution of activation enthalpy  $\Delta_r H^*$  values of as-milled  $\text{LaMg}_{11}\text{Ni} + x\% \text{Ni}$  ( $x=100, 200$ ) alloys with milling time

Moreover, it is very clear that, for all the milling time, the  $\text{LaMg}_{11}\text{Ni}+200\%\text{Ni}$  alloy always displays a lower  $\Delta_r H^*$  value than the  $\text{LaMg}_{11}\text{Ni}+100\%\text{Ni}$  alloy, which is considered to be responsible for the electrochemical kinetics improved by increasing Ni content.

Based on the above-mentioned results, we can conclude that extending milling time gives rise to a beneficial or harmful action on the electrochemical kinetics of the alloys. The positive impact is most likely ascribed to the following two aspects: Firstly, the mechanical milling fundamentally modifies the surface state of the alloy powder, and especially a great number of crystal defects are created, which are very beneficial to accelerate the charge transfer and hydrogen diffusion. Secondly, mechanical milling makes the sizes of the alloy powders dramatically decrease, increasing the interface area of the alloy particle surface and the electrolyte. As to the adverse effect incurred by milling, it is believed to be associated with the facilitated amorphous phase by increasing milling time since an amorphous phase can strongly prohibit the pulverization of the alloy during charge–discharge cycle [33], reducing available new surface of the alloy electrode, which impairs not only the charge transfer rate at the alloy/electrolyte interface but also the hydrogen diffusion ability.

#### 4 Conclusions

1) The nanocrystalline and amorphous  $\text{LaMg}_{11}\text{Ni}+x\%\text{Ni}$  ( $x=100, 200$ ) alloys were successfully synthesized by mechanical milling. With the Ni content increasing from 100% to 200%, the maximum discharge capacity of the as-milled alloys is enhanced from 192.9 to 1017.2  $\text{mA}\cdot\text{h/g}$  at a discharge current density of 60  $\text{mA/g}$ .

The maximum values of the  $D_{HR}$  of the as-milled  $\text{LaMg}_{11}\text{Ni}+x\%\text{Ni}$  ( $x=100, 200$ ) alloys are 72.6% and 75.2%. Furthermore, the potential characteristics of the as-milled alloys were markedly improved by increasing Ni content and prolonging milling time.

2) The gaseous hydrogen absorption capacities ( $C_{100}^a$ ) and kinetics ( $R_{10}^a$ ) of the as-milled alloys have maximum values with varying milling time, but hydrogen desorption kinetics ( $R_{20}^d$ ) always increases with milling time prolonging. This is attributed to the facilitated glass forming ability by increasing Ni content and the decreased hydrogen desorption activation energy by extending milling time.

3) Increasing Ni content significantly improves the gaseous and electrochemical hydrogen storage kinetics of the as-milled alloys, which is ascribed to the decreased hydrogen desorption activation energy and activation enthalpy caused by increasing Ni content.

## References

- [1] MORI D, HIROSE K. Recent challenges of hydrogen storage technologies for fuel cell vehicles [J]. *International Journal of Hydrogen Energy*, 2009, 34(10): 4569–4574.
- [2] CIPRIANI G, DIO V D, GENDUSO F, CASCIA D L, LIGA R, MICELI R. Perspective on hydrogen energy carrier and its automotive applications [J]. *International Journal of Hydrogen Energy*, 2014, 39(16): 8482–8494.
- [3] ZHANG Y H, CHEN L C, ZHAO C, YANG T, XU C, ZHAO D L. An investigation on electrochemical performances of as-cast and annealed  $\text{La}_{0.8}\text{Mg}_{0.2}\text{Ni}_{3.3}\text{Co}_{0.2}\text{Si}_x$  ( $x=0-0.2$ ) alloy electrodes for Ni/MH battery application [J]. *Journal of Central South University*, 2014, 21(6): 2125–2135.
- [4] SAKINTUNA B, LAMARI-DARKRIM F, HIRSCHER M. Metal hydride materials for solid hydrogen storage: A review [J]. *International Journal of Hydrogen Energy*, 2007, 32(9): 1121–1140.
- [5] O'MALLEY K, ORDAZ G, ADAMS J, RANDOLPH K, AHN C C, STETSON N T. Applied hydrogen storage research and development: A perspective from the U.S. department of energy [J]. *Journal of Alloys and Compounds*, 2015, 645: s419–s422.
- [6] UMEGAKI T, YAN J M, ZHANG X B, SHIOYAMA H, KURIYAMA N, XU Q. Boron- and nitrogen-based chemical hydrogen storage materials [J]. *International Journal of Hydrogen Energy*, 2009, 34(5): 2303–2311.
- [7] YANG T, YUAN Z M, BU W G, JIA Z C, QI Y, ZHANG Y H. Evolution of the phase structure and hydrogen storage thermodynamics and kinetics of  $\text{Mg}_{88}\text{Y}_{12}$  binary alloy [J]. *International Journal of Hydrogen Energy*, 2016, 41(4): 2689–2699.
- [8] ZHANG Y H, YANG T, BU W G, CAI Y, ZHANG G F, ZHAO D L. Effect of Nd content on electrochemical performances of nanocrystalline and amorphous  $(\text{Mg}_{24}\text{Ni}_{10}\text{Cu}_2)_{100-x}\text{Nd}_x$  ( $x=0-20$ ) alloys prepared by melt spinning [J]. *Transactions of Nonferrous Metals Society of China*, 2013, 23(12): 3668–3676.
- [9] ZHANG Y H, YANG T, ZHAI T T, YUAN Z M, ZHANG G F, GUO S H. Effects of stoichiometric ratio La/Mg on structures and electrochemical performances of as-cast and annealed La–Mg–Ni-based  $\text{A}_2\text{B}_7$ -type electrode alloys [J]. *Transactions of Nonferrous Metals Society of China*, 2015, 25(6): 1968–1977.
- [10] ZHANG Y H, XU S, ZHAI T T, YANG T, YUAN Z M, ZHAO D L. Hydrogen storage kinetics of nanocrystalline and amorphous Cu–Nd-added  $\text{Mg}_2\text{Ni}$ -type alloys [J]. *Transactions of Nonferrous Metals Society of China*, 2014, 24(11): 3524–3533.
- [11] CAPURSO G, NAIK M U D, RUSSO S L, MADDALENA A, SACCONI A, GASTALDO F, NEGRI S D. Study on La–Mg based ternary system for hydrogen storage [J]. *Journal of Alloys and Compounds*, 2013, 580: s159–s162.
- [12] ZHANG Y H, YANG T, ZHAI T T, SHANG H W, ZHANG G F, ZHAO D L. Influences of substituting Ni with M (M=Cu, Co, Mn) on gaseous and electrochemical hydrogen storage kinetics of  $\text{Mg}_{20}\text{Ni}_{10}$  alloys [J]. *Journal of Central South University*, 2014, 21(5): 1705–1713.
- [13] WIRTH E, MILCIUS D, FILIOU C, NORÉUS D. Exploring the hydrogen sorption capacity of Mg–Ni powders produced by the vapour deposition technique [J]. *International Journal of Hydrogen Energy*, 2008, 33(12): 3122–3127.
- [14] GU H, ZHU Y F, LI L Q. Effect of La/Ni ratio on hydrogen storage properties of Mg–Ni–La system prepared by hydriding combustion synthesis followed by mechanical milling [J]. *International Journal of Hydrogen Energy*, 2008, 33(12): 2970–2974.
- [15] LØKEN S, SOLBERG J K, MAEHLEN J P, DENYS R V, LOTOTSKY M V, TARASOV B P. Nanostructured Mg–Mm–Ni hydrogen storage alloy: Structure-properties relationship [J]. *Journal of Alloys and Compounds*, 2007, 446–447: 114–120.
- [16] RÉVÉSZ Á, GAJDICS M, VARGA L K, KRÁLLICS G, PÉTER L, SPASSOV T. Hydrogen storage of nanocrystalline Mg–Ni alloy processed by equal-channel angular pressing and cold rolling [J]. *International Journal of Hydrogen Energy*, 2014, 39(18): 9911–9917.
- [17] WANG Y, QIAO S Z, WANG X. Electrochemical hydrogen storage properties of ball-milled  $\text{NdMg}_{12}$  alloy with Ni powders [J]. *International Journal of Hydrogen Energy*, 2008, 33(3): 1023–1027.
- [18] ZHANG Q A, JIANG C J, LIU D D. Comparative investigations on the hydrogenation characteristics and hydrogen storage kinetics of melt-spun  $\text{Mg}_{10}\text{NiR}$  (R=La, Nd and Sm) alloys [J]. *International Journal of Hydrogen Energy*, 2012, 37(14): 10709–10714.
- [19] POLETAEV A A, DENYS R V, MAEHLEN J P, SOLBERG J K, TARASOV B P, YARTYS V A. Nanostructured rapidly solidified  $\text{LaMg}_{11}\text{Ni}$  alloy: Microstructure, crystal structure and hydrogenation properties [J]. *International Journal of Hydrogen Energy*, 2012, 37(4): 3548–3557.
- [20] ABDELLAOUI M, MOKBLI S, CUEVAS F, LATROCHE M, PERCHERON-GUÉGAN A, ZARROUK H. Structural and electrochemical properties of amorphous rich  $\text{Mg}_x\text{Ni}_{100-x}$  nanomaterial obtained by mechanical alloying [J]. *Journal of Alloys and Compounds*, 2003, 356–357: 557–561.
- [21] DENYS R V, POLETAEV A A, SOLBERG J K, TARASOV B P, YARTYS V A.  $\text{LaMg}_{11}$  with a giant unit cell synthesized by hydrogen metallurgy: Crystal structure and hydrogenation behavior [J]. *Acta Materialia*, 2010, 58(7): 2510–2519.
- [22] TERESIAK A, GEBERT A, SAVYAK M, UHLEMANN M, MICKEL C H, MATTERN N. In situ high temperature XRD studies of the thermal behaviour of the rapidly quenched  $\text{Mg}_{77}\text{Ni}_{18}\text{Y}_5$  alloy under hydrogen [J]. *Journal of Alloys and Compounds*, 2005, 398(1): 156–164.
- [23] ANIK M, KARANFIL F, KÜÇÜKDEVECİ N. Development of the high performance magnesium based hydrogen storage alloy [J]. *International Journal of Hydrogen Energy*, 2012, 37(1): 299–308.
- [24] SADHASIVAM T, HUDSON M S L, PANDEY S K, BHATNAGAR A, SINGH M K, GURUNATHAN K. Effects of nano size mischmetal and its oxide on improving the hydrogen sorption behaviour of  $\text{MgH}_2$  [J]. *International Journal of Hydrogen Energy*, 2013, 38(18): 7353–7362.
- [25] KISSINGER H E. Reaction kinetics in differential thermal analysis [J]. *Analysis Chemistry*, 1957, 29(11): 1702–1706.

- [26] WU Y, HAN W, ZHOU S X, LOTOTSKY M V, SOLBERG J K, YARTYS V A. Microstructure and hydrogenation behavior of ball-milled and melt-spun Mg–10Ni–2Mm alloys [J]. Journal of Alloys and Compounds, 2008, 466(1–2): 176–181.
- [27] XIE D H, LI P, ZENG C X, SUN J W, QU X H. Effect of substitution of Nd for Mg on the hydrogen storage properties of Mg<sub>2</sub>Ni alloy [J]. Journal of Alloys and Compounds, 2009, 478(1–2): 96–102.
- [28] SONG M Y, YIM C D, KWON S N, BAE J S, HONG S H. Preparation of Mg<sub>23.5</sub>Ni<sub>10</sub> (Cu or La) hydrogen-storage alloys by melt spinning and crystallization heat treatment [J]. International Journal of Hydrogen Energy, 2008, 33(1): 87–92.
- [29] ANIK M. Electrochemical hydrogen storage capacities of Mg<sub>2</sub>Ni and MgNi alloys synthesized by mechanical alloying [J]. Journal of Alloys and Compounds, 2010, 491(1–2): 565–570.
- [30] ZHAO X Y, DING Y, MA L Q, WANG L Y, YANG M, SHEN X D. Electrochemical properties of MmNi<sub>3.8</sub>Co<sub>0.75</sub>Mn<sub>0.4</sub>Al<sub>0.2</sub> hydrogen storage alloy modified with nanocrystalline nickel [J]. International Journal of Hydrogen Energy, 2008, 33(22): 6727–6733.
- [31] ZHANG G, POPOV B N, WHITE R E. Electrochemical determination of the diffusion coefficient of hydrogen through an LaNi<sub>4.25</sub>Al<sub>0.75</sub> electrode in alkaline aqueous solution [J]. Journal of the Electrochemical Society, 1995, 142(8): 2695–2698.
- [32] KURIYAMA N, SAKAI T, MIYAMURA H, UEHARA I, ISHIKAWA H, IWASAKI T. Electrochemical impedance and deterioration behavior of metal hydride electrodes [J]. Journal of Alloys and Compounds, 1993, 202(1–2): 183–197.
- [33] ZHANG Y H, YUAN Z M, YANG T, QI Y, ZHAO D L. Effect of mechanical grinding on the electrochemical hydrogen storage properties of Mg–Ni–Y alloy [J]. Journal of Solid State Electrochemistry, 2015, 19(4): 1187–1195.

## 球磨制备 La–Mg–Ni 基 LaMg<sub>12</sub> 型 纳米晶–非晶合金的储氢性能

张羊换<sup>1,2</sup>, 李龙文<sup>1,2</sup>, 冯佃臣<sup>1,3</sup>, 宫鹏飞<sup>1,2</sup>, 尚宏伟<sup>2</sup>, 郭世海<sup>2</sup>

1. 内蒙古科技大学 内蒙古自治区白云鄂博矿多金属资源综合利用重点实验室, 包头 014010;
2. 钢铁研究总院 功能材料研究所, 北京 100081;
3. 北京科技大学 材料科学与工程学院, 北京 100083

**摘要:** 采用球磨方法制备 LaMg<sub>11</sub>Ni + x% Ni (x=100, 200) 纳米晶–非晶合金, 并利用自动恒电流系统测试合金的电化学储氢性能。使用附带测氢仪的差热分析(DSC)和 Sievert's 设备研究合金的气态储氢性能。实验结果表明, Ni 含量的增加能显著改善球磨合金的气态及电化学储氢性能。球磨合金的气态吸氢量和吸氢速率随着球磨时间的增加出现最大值。但合金的放氢动力学性能随着球磨时间的增加一直增加。另外, 球磨合金的放电容量和高倍率放电性能( $D_{HR}$ )都随球磨时间的增加先增加后减小。

**关键词:** Ni/MH 电池; 贮氢合金; 机械合金化; 放电容量; 动力学

(Edited by Yun-bin HE)